Journal of Materials Chemistry B

Accepted Manuscript

ROYAL SOCIETY OF CHEMISTRY

www.rsc.org/materialsB

Facile synthesis of N-halamine-labeled silica–polyacrylamide multilayer core–shell nanoparticles for antibacterial ability

Qiaohua Qiu, [a] Tao Liu, [ab] Zhihui Li, [a] Xinbo Ding [*a]

[a]College of Materials and Textiles, Zhejiang Sci-Tech University, Hangzhou 310018, China.

[b]Keyi College, Zhejiang Sci-Tech University, Hangzhou 311121, China.

[*] **Corresponding author**

Xinbo Ding, Ph.D., Associate Professor

Tel: +86-571 86843260; Fax: +86-571 86843255.

E-mail: dxblt@zstu.edu.cn (X. Ding).

Abstract:

The silica–polymer antimicrobial composites with core–shell nanostructure are often prepared through polymeric process. However, it is difficult to control the polymerization degree of the polymers to give a uniform size distribution. In this article, we present a facile approach to produce the antimicrobial silica@polyacrylamide (SiO_2@PAM) core–shell nanoparticles, which were synthesized via electrostatic self-assembly method using acyclic N-halamine polymeric polyacrylamide. The morphologies and structures of these as-prepared nanoparticles were characterized by different techniques. And their antibacterial performance against both gram-positive bacteria and gram-negative bacteria were also evaluated. Based on the preliminary results, these core–shell nanosized spheres were made of outer polymer shell-decorated inner SiO_2 core, where the encapsulation of silica nanoparticles with PAM polymers. After chlorination, resultant nanosized particles displayed powerful and stable bactericidal capability toward both two model bacteria. Bactericidal assessment further suggested the coordinated effects of the well-known antibacterial performance of N-halamines and the flocculation of PAM on antibacterial behavior. The *in vitro* cytotoxicity of the prepared nanoparticles with varying concentrations was studied using mouse fibroblasts cells (L929). The CCK-8 assay revealed that SiO_2@PAM composites possessed non-cytotoxic and favorable responses of seeded cells *in vitro*. These results indicate the suitability of SiO_2@PAM composites particles in controlling the biocidal activity, demonstrating their potential application for deactivating bacteria or even disease control.

Keywords: Silica-polymer; Core–shell nanoparticles; Electrostatic self-assembly; Antibacterial activity;

1. Introduction

The increasing bacterial infections become a major source of global public health risk. Considering the health care, the studies have directed the research agenda toward the design of new and effective antibacterial agents.[1]

Among them, N-halamine compounds proven to be a potent antimicrobial agent have been widely applied in various fields.[2–4] Compared with inorganic halogens, N-halamine polymers containing one or more nitrogen-halogen covalent bond exhibit several inherent features such as long-term stability, high durability, and regenerability.[5–7] Here N-Halamine materials act as biocides through the direct contact of microbial cells with oxidative halogen.[8,9] When bacteria contact with N-halamines, the halogen exchange reaction occurs, thereby causing the expiration of the cells. [10] In fact, the antibacterial performance of N-halamines as contact biocides strongly depends on their activated surface area, and thus the N-halamines in the nanometer-size regime show superior antibacterial activity due to their smaller size and larger surface area.[11–13] Most studies have utilized nanoparticles such as silica, iron oxide, carbon, and polymer as support to enhance the activated surface.[14] This strategy of introducing these nanostructures as template successfully enhanced the activated surface, and all these N-halamine-functionalized nanoparticles possessed improved antibacterial feature against both gram-positive and gram-negative bacteria compared with their bulk powder counterparts.

Of these templates, silica nanoparticles are the most ideal candidate as they are biocompatible, chemically inert, optical transparent, optimistically water dispersible, nontoxic to humans and environmentally friendly.[15–17] More importantly, the surface functions as the silanol groups on the surface offer versatile possibilities for covalently functionalizing the silica-coated particles.[18,19] Owing to these attractive features, developing silica-based carrier systems with the morphology and size governable nanoarchitectures is of chief interest. Actually, silica nanoparticles-based core–shell carriers have attracted intensive attention due to their wide applications in the field of catalysis, bioimaging and biolabeling, artificial cells, controlled-release delivery.[20] Thus, the exploration of silica nanopariticles-based core–shell carrier systems where the incorporatinon of silica nanoparticles into polymeric N-halamine matrices is currently under intensive research. In comparison with either pristine core or shell components, the silica-based core–shell carrier systems

combine multifarious properties in one entity consisting of different chemical components. The fabrication route to well-defined core–shell antimicrobial composites highlight the encapsulation of silica core nanoparticles with polymers, whereby the surface characteristics of the cores are modified by coating with a polymer layer.[21,22] The most common polymers used as organic coatings on silica cores are poly(methylmethacrylate) (PMMA), poly(vinyl acetate) (PVA), and polystyrene (PS).[23–26] Usually, the information of polymeric N-halamine was carried out by introducing vinyl monomers (*i.e.*, methyl methacrylate, vinyl acetate, and styrene) to copolymerize with N-halamine monomer on the surface of silica templates. However, the polymerization method often has the difficulty in controlling the polymerization degree of the polymers to give a uniform size distribution.

In this contribution, we developed a simple method to fabricate N-halamine-labeled core–shell silica–polymeric polyacrylamide using LbL electrostatic self-assembly process by two-stage process. First, monodisperse silica nanoparticles as the core was skillfully synthesized by sol-gel method based on the hydrolysis of tetraethoxysilane (TEOS). In this regard, silica nanopartilces could be used as supports to enhance the activated surface, thus yielding the improved antibacterial performance. Second, considering the existence of silanol groups on the surface, the surface of silica nanopartilces was coated using LbL electrostatic self-assembly technique by stepwise dipping the silica nanoparticles into a solution of cationic polyacrylamide (CPAM) and anionic polyacrylamide (APAM). Differ from previous polymerization technique, this study attempts developing for the first time two cationic and anionic PAMs coating on silica cores to form stable SiO_2@PAM multilayer core–shell nanoparticles. After treatment with bleaching, the amines groups in polymer shell were transformed into N-halamine structures to obtain N-halamine-labeled silica–polyacrylamide core–shell nanoparticles. Herein the morphology, structure, and physic-chemical characterization of SiO_2@PAM nanoparticles were analyzed, and the antimicrobial performance of the as-synthesized products

was also evaluated by selecting Staphylococcus aureus (*S. aureus*) and Escherichia coli (*E. coli*) as the typical microorganisms. Subsequently, the final effects on the cytotoxicity ability were carried out to test the cell viability using mouse fibroblast L929 as model.

2. Experimental details

2.1 Materials

TEOS was obtained from Tianjin Chemical Kemiou Reagent Co., Ltd. Ethanol, ammonia hydroxide (28% in water) and sodium hypochlorite (5 wt%) were purchased from Hangzhou Gaojing Fine Chemical Research Institute. CPAM (M_w ~12,000,000) and APAM (M_w ~12,000,000) were available from Aladdin. Peptone, nutrient agar and yeast were biochemical reagents. The reagents were analytical grade and used without any purification.

2.2 Preparation of silica–polymer core–shell nanoparticles

The preparation of SiO_2@PAM core–shell nanoparticles was achieved via LbL electrostatic self-assembly through the following two steps, as shown in Fig. 1.

Step 1: the fabrication of SiO_2 nanoparticles. Relying on the well-known stöber process,[27] TEOS was added dropwise into a mixture solution containing 50 mL of ethanol, 1.0 mL of deionized water, and 3.0 mL of ammonia hydroxide. Then the above mixture was stirred vigorously for 4 h at room temperature, thereby offering monodisperse silica nanoparticles.

Step 2: LbL electrostatic self-assembly process. Accordingly, about 200 mg of CPAM was added into the solution. After stirring for 2 h, 200 mg APAM was dipped into the above mixture for 2 h to undergo the electrostatic self-assembly process. After that, the obtained SiO_2@PAM core–shell nanoparticles were purified

by centrifugation (10,000 rpm, 10min) and re-dispersed in deionized water several times.

2.3 Chlorination of SiO_2@PAM core–shell nanoparticles

The as-prepared SiO_2@PAM core–shell nanoparticles were dispersed into 10% commercial aqueous sodium hypochlorite solution (0.5% NaClO) by stirring for 2 h at pH = 7.0. To remove the free oxidative chlorine absorbed on the surface of silica nanoparticles, the chlorinated samples were washed thoroughly with distilled water and dried at 60 ℃ for 1 h. The chlorinated SiO_2@PAM nanoparticles were denoted as SiO_2@PAMC.

2.4 Physicochemical characterizations

The morphologies and microstructures of these samples were observed using the field-emission scanning electron microscopy (FESEM; Ultra-55, Carl Zesis), and transmission electron microscopy (TEM; JEM2100, JEOL). Thermogravimetric analysis (TGA) was performed by Perkin Elmer thermogravimetric analyzer at the heating rate of 10 ℃/min ranging from room temperature to 800 ℃ under nitrogen atmosphere. The thermal properties of the samples were carried out through the Perkin Elmer DSC 8000 at the heating rate of 10 ℃/min under nitrogen atmosphere. The optical absorption spectra in the ultraviolet and visible region were investigated through Spectrophotometer Lambda 900 in the wavelength from 200 to 1000 nm. Fourier transitioned infrared spectroscopy (FTIR) were collected on Nicolet FTIR 5700.

2.5 Bacterial culture

To evaluate the antibacterial activity of the samples, *S. aureus* (ATCC 6538) and *E. coli* (ATCC 8739) were chosen as the models for the gram-positive bacteria and gram-negative bacteria, respectively. Bacteria were grown overnight at 37 ℃ under agitation in Luria Bertani (LB) growth medium. Bacterial cells at the exponential growth phase were harvested by centrifugation, washed twice with phosphate-buffered saline

(PBS), and then diluted to concentrations of ~2×10^5 colony-forming units (CFU) per mL.

2.6 Antibacterial assessment

The antibacterial activity of these synthesized nanoparticles was assessed against gram-positive and gram-negative bacteria. Before the antibacterial test, glassware was sterilized by autoclave at 120 ℃ for 1.5 h. Accordingly, the test samples were sterilized by ultraviolet (UV) light for 30 min. To determine the antibacterial activity, 100 mg of each sample was dispersed into a conical flask containing 47.5 mL of phosphate-buffered saline solution and 2.5 mL nutrient broth inoculated with ~2×10^5 CFU per mL of bacteria. The solutions were incubated in a shaking incubator at 37 ℃ overnight. After that, 0.1 mL of the mixture was dispersed into the nutrient agar plate and incubated at 37 ℃ for 24 h. Photographs of *S. aureus* and *E. coli* colonies grown on agar plates were obtained to assess their antibacterial performance. And the number of colonies was counted to calculate the antibacterial activity. Each trial was carried out in triplicate, and the means were reported for all the independent experiments. Especially, the antibacterial rate of SiO_2@PAMC sample is determined using the following the equation: Antibacterial ratio (%) = $\left[\left(N_{control}-N_{sample}\right)/N_{control}\right]\times100$, where $N_{control}$ and N_{sample} represent the numbers of surviving bacterial colonies from the control and the test groups, respectively.

2.7 Turbidity assay

LB liquid medium turbidity assays were employed to evaluate antibacterial activities towards *E. coli* and *S. aureus*. 0.5 mL of bacteria suspension was added into 4.5 mL culture solution and mixed well under constant shaking. 100 mg of each sample (pure SiO_2、SiO_2@PAM、SiO_2@PAMC) was placed in glass tubes with above suspension and then diluted to an appropriate concentration. The glass tubes were incubated in a shaking incubator at 37 ℃. Afterwards, 0.1 mL liquids were withdrawn from the tubes at different incubation times

(*e.g.*, 0, 2, 4, 6, 8, 10, 12, 14, 18, and 24 h). After incubation period of 24 h, the turbidity photographs of the test tubes were observed to estimate their antibacterial activity. The turbidity formed after incubation period of different times was measured by the optical density at 600 nm (OD_{600}, which is well recognized as the characteristic peak for determining the bacterial number) using a microplate reader (Bio-Rad 680, USA). The bacterial growth kinetics of the test nanoparticles under different contact time was measured to quantitatively evaluate the antibacterial activity.

2.8 The long-term stability of SiO_2@PAMC

To study the stability, SiO_2@PAMC core–shell nanoparticles were stored at room temperature for two months. After that, their antibacterial performances against *S. aureus* were estimated as a function of contact time (*e.g.*, 5, 15, 30 and 60 min). As for antibacterial kinetic test, 100 mg of test sample (*i.e.*, SiO_2@PAMC nanoparticles before and after two month storage) was dispersed into a glass tube containing 4.5 mL culture solution and 0.5 mL bacteria suspension. Then, the above-mentioned sample suspension was immersed in a shaking incubator at 37 ℃. The resulting mixture was mixed well, serially diluted, and then 100 μL of each dilution was dispersed onto LB agar plates under different contact time (5, 15, 30 and 60 min). The photographs of colonies on the plates were obtained after incubation at 37 ℃ for 24 h. The fractional survival of SiO_2@PAMC nanoparticles before and after two month storage was measured at different contact time.

2.9 Cell culture and cytotoxicity

Mouse fibroblast L929 cells were used to evaluate the possible cytotoxicity of the test nanoparticles by a CCK-8 (Dojindo, Japan) assay. L929 cells were pre-incubated in a 96-well plate (1×10^5 cells per well) with cultured in dulbecco's modified eagle medium (DMEM, Gibco) supplemented with 10% fetal bovine serum

(FBS, Gibco) at 37 ℃ in a humidified atmosphere with 5% CO_2. The synthesized nanoparticles (SiO_2, SiO_2@PAM, and SiO_2@PAMC) were soaked in ethanol (75% v/v) and sterilized using UV light followed by washing with sterile phosphate-buffered saline (PBS, pH 7.4). The cells were further incubated with these nanoparticles with six concentrations, 50 μg/mL, 100 μg/mL, 200 μg/mL, 300 μg/mL, 400 μg/mL and 500 μg/mL for 72 h. Subsequently, 10 μL CCK-8 reagents solution was added to each well, followed by incubation at 37 ℃ for 4 h. The optimal images of the samples/cell constructs were observed under a microscope at 20× magnification. The absorbance of the supernatant was measured at 450 nm using a microplate reader (SpectraMax M5, Molecular Devices, USA). Each experiment was independently performed at least three times. The cells treated with 10 mL of PBS were used as a negative control and the relative cell viability was calculated as follows: $\text{OD ratio (\%)} = \left[\left(OD_{sample} - OD_{blank}\right) / \left(OD_{control} - OD_{blank}\right)\right] \times 100$. The results were expressed as mean ± standard deviation (mean ± SD). Statistical analysis was carried out using one-way ANOVA, and differences of $p < 0.05$ were considered to be statistically significant.

3. Results and discussion

3.1 Characterization of the SiO_2@PAM core–shell nanoparticles

TEM and FESEM images (Fig. 2) show the morphology, shape, surface state and size distribution of pure SiO_2 and SiO_2@PAM core–shell nanoparticles. Fig. 2a presents a typical TEM image of SiO_2 nanoparticles. The obtained quasi-monodisperse SiO_2 nanoparticles had legible spherical shape, consisting of a compacted center and a relatively loose edge. Each of the SiO_2 nanoparticles appeared slightly darker near the center and lower at the edges. In Fig. 2b, pure SiO_2 nanoparticles displayed a spherical shape with smooth and intact surface. Unlike silica nanoparticles, the obtained SiO_2@PAM core–shell nanoparticles had legible spherical shape and obvious multilayer structure, implying the existence of the PAMs coating outside the silica core. Besides, the

strong contrast difference in the prepared nanoparticles with a dark inner center and relatively light edge further confirmed the successful encapsulation of SiO_2 nanoparticles with polymers (Fig. 2d). Centered on the negatively charged SiO_2 nanoparticles, the deposition of polymer by the introduction of CPAM and APAM in turn appeared on the silica cores in the LbL electrostatic self-assembly process, affording stable silica–PAM core–shell nanoparticles. Therefore, two-layers continuous PAM polymer shell can be clearly observed on the outer surface of SiO_2 core. The shell thickness of PAM polymer showed the size of spherical shape at a diameter of approximately 40 nm (Fig. 2d). The FESEM micrograph of SiO_2@PAM samples presented relatively smooth particle surface with similar sphere shape, as shown in Fig. 2e. It is found that no significant differences were observed on the morphology of them. The size distribution of SiO_2 and SiO_2@PAM core–shell nanoparticles is given as well in Fig. 2c and f. Both two nanoparticles with spherical morphology exhibited unimodal and narrow particle size distribution, ranging from 220 to 310 nm and from 325 to 450 nm. According to dynamic light scattering (DLS) measurement, the particle size for SiO_2 and SiO_2@PAM core–shell nanoparticles were 263.5 ± 54.2 and 367.1 ± 95.8 nm, respectively. Obviously, the deposition of PAM polymers on the silica core increased the size distribution of SiO_2@PAM nanoparticles, which is well agreed with those polymerization method previous reported.[15,28,29] This phenomenon further confirmed the successful encapsulation of SiO_2 nanoparticles with PAM polymers, just as observed in Fig. 2d and e. The fabrication of SiO_2@PAM core–shell samples reflected this LbL electrostatic self-assembly approach is feasible. Moreover, the particle size of as-synthesized core–shell nanoparticles will be tailored by tuning the experimental parameters such as particle size of the silica core, shell concentration, and shell thickness. By understanding these controllable parameters, we can engineer the core–shell nanoparticles with the required core and shell size for optimal application performance.

DSC curves of pure SiO_2 and SiO_2@PAM nanoparticles are shown in Fig. 3. It is observed that pure SiO_2

nanoparticles showed only one smooth line without glass transition temperature, melting points and crystallization transitions, which is a typical characteristic of the inorganic materials. However, a transition temperature ranging from 198 to 205 ℃ appeared in the DSC curves of SiO_2@PAM nanoparticles, corresponding to the melting points of PAM. The observations in the DSC curves of SiO_2@PAM sample indicated the successful encapsulation of silica nanoparticles with PAM polymer.

TG analysis results are shown in Fig. 4. On TG curves, different stages were found with the increment of temperature. For CPAM, the total weight loss can be roughly divided into three regions. The first mass loss occurred at the initial stage of heating within the range of 30–220 ℃, which was assigned to the adsorbed water and residual organic solvent elimination in the systems.[30] When the temperature was further increased, the second mass was recorded in the range of 220–340 ℃, ascribing to the evolution of NH_3. The third weight loss at above 340 ℃ was accompanied with main chain scission process.[31,32] In the case of SiO_2@PAM core–shell nanoparticles, it is noteworthy that the mass loss observed in the TGA curves occurred in three distinct steps. The first weight loss of approximately 10.9 % occurred at below 238 ℃ was attributed to the removal of desorbed water and residual organic solvent. With increasing the temperature, the second mass decrease of 3.4 % was recorded in the range of 238–360 ℃, corresponding to the NH_3 evolution from CPAM. However, after the introduction of APAM into the composites the thermal decomposition temperature from TG curves was different from that of CPAM sample. Within the temperature region of above 360 ℃, the mass loss (about 7.2%) was associated with the NH_3 evolution from APAM and the main chain scission of CPAM. After the isothermal heating, the incombustible residues remaining after pyrolysis were assumed to be pure silica. Compared with TG curves of CPAM and pure SiO_2 samples, these observations from the as-prepared particles further confirmed the immobilization of PAM as the shell on the surface of silica core.

Another evidence for the presence of PAM on the silica surface can be obtained from the FTIR

spectroscopy. Fig. 5 shows the FTIR spectra of SiO_2, SiO_2@PAM, SiO_2@PAMC nanoparticles compared with CPAM sample. The vibrational peaks at approximately 3440, 2920, and 1640 cm^{-1} in the CPAM sample were associated with the N–H stretching vibration, the C–H stretching vibration, and the stretching vibration of amide C=O (–$CONH_2$), repectively.[33,34] Specially, amide groups with two possible accepting sites (*i.e.*, the nitrogen atom and the carbonyl group) often suggested the hydrogen bonding which mainly takes place with the carbonyl group.[35] For other three samples, the FTIR data regarding the structure of the silica matrix indicated that a broad band between 1000 and 1300 cm^{-1}, composed of an intense peak attributed to Si–O–Si asymmetric stretching mode at 1100 cm^{-1}, and a shoulder identified as Si−O−Si stretching mode at 1230 cm^{-1}. The band at 950 cm^{-1} was ascribed to the Si–O–H stretching vibration. Additionally, the bending Si–O–Si vibration was observed around 802 cm^{-1}, described as characteristic of ring structures in the silica matrix.[36,37] These peaks mentioned above were observed in the curves of SiO_2@PAM sample, as shown in Fig. 5. Interestingly, two resolved peaks around 3440 and 3390 cm^{-1} were observed on the SiO_2@PAM sample. The appearance of absorption peak occurred at 3390 cm^{-1} was attributed to the stretching vibration of intermolecular hydrogen bonds between N–H and C=O.

After treatment with regular chlorine bleaching, the amide groups of the N–H bonds are readily transformed into N–Cl groups to form N-halamine structures. Such this transformation can be observed with the FTIR spectra of SiO_2@PAM and SiO_2@PAMC samples. Compared with SiO_2@PAM sample, the peak located at 3390 cm^{-1} disappeared in the FTIR spectrum of SiO_2@PAMC sample. After chlorination, the amide groups from the PAM were transformed into N-halamine structures, associating with the breakage of hydrogen bonds between N–H and C=O.[23] These evident differences between the chlorinated and unchlorinated samples strongly suggested that the amide groups were transformed into N-halamine structures. On the other hand, the formation of characteristic bands in the core–shell particles, such as N–H, C=O, and Si–O–Si, also

demonstrated the PAM copolymer can be deposited on the surface of the silica nanoparticles by the LbL electrostatic self-assembly.

To further investigate the structure in these materials, UV-vis absorption spectra of pure SiO_2, SiO_2@PAM, and SiO_2@PAMC samples are shown in Fig. 6. It is worth noted that the bands at ~300, 410 nm assignable to the characteristic absorption bands of Si–O–Si were observed in all samples. In the case of pure SiO_2 sample, the absorption band at 520 nm was assigned to the presence of the Si–O–H in the structure. For SiO_2@PAM sample, a new absorption band between 572 and 607 nm corresponding to the N–H···N–H hydrogen bonding was detected, and a wide absorption band in the region 410 ~ 490 nm was also shown in the UV-vis spectra. And the absorption band at 450 nm was attributed to the C=O group, while the bands from 450 to 490 nm can be belong to the N–H···O=C hydrogen bonding. Comparatively, another peak centered at 520 nm assignable to the Si–O–H band was vanished in the UV-vis spectra of SiO_2@PAM sample. These differences between pure SiO_2 and SiO_2@PAM sample implied that the existence of the PAM coating outside the silica core.

After bleaching, the maximum value of this peak at 607 nm in unchlorinated sample shifted to 572 nm in chlorinated sample, which might be attributed to the amide groups from the PAM. Moreover, the absorption band at 490 nm was also disappeared in UV-vis absorption spectrum. This structural variation were directly correlated with the transformation of N–H bonds to N–Cl groups, resulting in the breakage of N–H···O=C and N–H···N–H hydrogen bonding. The behavior was in accordance with that testified by FTIR measurements as shown in Fig. 5.

3.2 Antibacterial properties

The antibacterial feature of SiO_2, SiO_2@PAM, and SiO_2@PAMC particles is evaluated by measuring their ability against both *S. aureus* and *E. coli* bacteria. Fig. 7a presents the photographs of colonies of bacteria incubated on agar plates. There were signicant differences in antibacterial effects between the samples.

Typically, both the *E. coli* and *S. aureus* cells grew very well for the SiO_2 group, which can be easily observed by the bacterial lawn on the corresponding agar plates of the photograph. In the case of the SiO_2@PAM group, the bacterial colonies presented a visible reduction after the contact with the PAM-coated silica nanoparticles. In marked contrast, there are barely any bacterial lawn of *E. coli* and *S. aureus* growing on the corresponding agar plates compared with the other two groups, suggesting the visible growth reduction of *E. coli* and *S. aureus* cells induced by the N-halamine-functionalized SiO_2@PAMC sample. Moreover, the number of remaining bacteria was examined to determine the degree of the antibacterial effect in the presence of the antibacterial material. The number of surviving bacteria was estimated by counting the exact number of colonies, as shown in Fig. 7b. No significant reduction of the bacterial colonies was observed between SiO_2 and SiO_2@PAM groups. In marked contrast, fewer colonies were formed on the agar plates after the exposure to the SiO_2@PAMC. Meanwhile, the antibacterial rate of SiO_2@PAMC against *E. coli* and *S. aureus* was 95.5% and 96.2%, respectively. It was confirmed that SiO_2@PAMC core–shell nanoparticles were effective in reducing the bacterial growth among these groups.

Besides, the antibacterial property of the prepared nanoparticles is assessed via LB liquid medium turbidity assay. The photographs of the test tubes showing difference in turbidity were shown in Fig. 8(a, b). Usually, more turbidity is correlated to the higher bacterial growth whereas the clear solution shows lower bacterial growth. In the present study, the SiO_2 and SiO_2@PAM groups became turbid at 24 h incubation, indicating rapid growth of bacteria in the culture system. In marked contrast, the test tubes containing SiO_2@PAMC materials markedly inhibited the growth of *E. coli* and *S. aureus*, producing a clearly pellucid observation in the test tubes. It is reasonable to postulate that SiO_2@PAMC nanoparticles afforded preferable antibacterial activities on inhibiting bacterial proliferation due to the enhanced antibacterial activity from N-halamines structure. On the other hand, the bacterial growth curves in LB liquid media further confirmed that

the test tubes having SiO_2@PAMC nanoparticles showed significant reduction in bacterial growth against both *E. coli* and *S. aureus.* Fig. 8(c, d) shows OD measurement data of antibacterial activity study against *E. coli* and *S. aureus* at different incubation times (*e.g.*, 0, 2, 4, 6, 8, 10, 12, 14, 18, and 24 h). In terms of SiO_2 and SiO_2@PAM groups, the normal growth characteristics of *E. coli* bacterials were observed in 24 h of culture period. For SiO_2@PAM groups, *E. coli* cells presented exponential growth with the increase of incubation time, thus resulting in the maximum concentration of 0.72 OD after 14 h incubation (red line in Fig. 8c). Notably, the SiO_2@PAMC sample achieved a relatively low cell concentration of 0.13 OD after 24 h incubation (blue line in Fig. 8c), demonstrating that the proliferation of *E. coli* cells was efficiently inhibited by the SiO_2@PAMC. As shown in Fig. 8d, the SiO_2@PAM samples failed to inhibit the growth of *S. aureus* cells, reaching the maximum cell concentration of 0.72 OD after 18 h incubation, whereas the SiO_2@PAMC exhibited a low level of the OD value (~0.12) under the same conditions. These observations collectively suggested that SiO_2@PAMC nanoparticles showed significant reduction in bacterial growth against both *S. aureus* and *E. coli*. It means that after the chlorination treatment the presence of N-halamines in the SiO_2@PAMC nanoparticles could be responsible for the enhanced antibacterial activity.

Long-term stability is an important feature of N-halamine based antibacterial materials.[38] In this regard, the SiO_2@PAMC was stored at room temperature for two months to study the stability, and the antibacterial kinetic test as a function of contact time was studied to assess their antibacterial performances. Fig. 9(a–e) gives the photographs of the *S. aureus* bacterial culture plates after the exposure to the control and SiO_2@PAMC under different contact time. It is found that dense bacterial colonies were observed on the control plate, and significant reduction of the bacterial colonies was detected upon a 5 min exposure. In general, bacterial survival decreased with prolonged contact time. When the contact time extended from 15 min to 60 min, the small white dots decreased remarkably. Consequently, few survival bacterial colonies

existed on the culture plate after the contact time reached 60 min. As expected, the SiO_2@PAMC nanoparticles before storage at different contact time also proved that bacterial survival decreased with the extending contact time (Fig. S1†). Fig. 9f quantificationally illustrates the fractional survival of *S. aureus* upon the exposure to SiO_2@PAMC nanoparticles before and after two month storage. Regardless of the SiO_2@PAMC nanoparticles before and after storage, the fractional survival of the bacteria decreases drastically with the increase of contact time. Before storage, the control group (blank solution) showed 100% fractional survival. After *S. aureus* upon the exposure to SiO_2@PAMC nanoparticles, the fractional survival shifted to 40% with a contact time of 5 min. The increase in contact treatment, the further reduction of the fractional survival was ranging from 30 % to 19 %. Especially, the SiO_2@PAMC nanoparticles executed almost the whole *S. aureus* even after the contact time of 60 min. The decrease in the fractional survival indicated contact time is one of the major factors in killing the microorganisms. However, the SiO_2@PAMC nanoparticles after storage still possessed the similar trend curve compared with the sample before storage. The fractional survival of the *S. aureus* bacteria corresponding to each contact time was close to that value before two month storage. More importantly, there was no significant reduction in biocidal activity even after two months storage, implying that the strong and stable antibacterial activity of the obtained SiO_2@PAMC nanoparticles in the dry state.

Taking into consideration the antibacterial mechanism, Li *et al*. had found that the direct transfer of oxidative chlorine from amine N-halamine nanoparticles to the pathogen bacteria (contact mechanism) was seemed to be more favorable than the dissociation of positive halogen from N–Cl bond into solution with subsequent inactivation (release mechanism).[29] In this study, PAM as a kind of polymer flocculants showed an excellent absorption bridging effect, which was widely applied to water treatment and textiles. Kocer *et al.* reported a new N-halamine acrylamide monomer having 31 wt.% chlorine loading capability was synthesized

and then copolymerized with a tethering siloxane monomer. The resulting chlorinated copolymers on cotton fabric inactivated about 8-logs of both gram-negative and gram-positive bacteria within 5–10 min.[39] Once the silica core nanoparticles were encapsulated with polymers, the obtained SiO_2@PAM nanoparticles exhibited a certain degree of antibacterial properties, owing to the high efficient flocculated property of PAM. When treated with bleaching, the improved antibacterial performance of SiO_2@PAMC nanoparticels arised from the N-halamine structures, leading to the obviously sparse colony in SiO_2@PAMC sample. Further research on the SiO_2@PAM core–shell will be conducted through coating them onto fabric to assess their antimicrobial effects.

3.3 Biocompatibility

Considering the effect of prepared nanoparticles on the cell reponse, mouse fibroblast L929 cells was cultured on these samples to evulate the *in vitro* biocompatibility. After seeding on material, OD ratio of L929 cells were determined by measuring the optical density (absorbance at 450 nm) using a CCK-8 assay. The cells were incubated with these nanoparticles for 72 h at various concentrations from 50 to 500 μg/mL. Fig. 10a shows the obtained OD ratio upon exposure to these nanoparticles with different concentrations for 72 h. For SiO_2@PAMC nanoparticles, the OD ratio increased with increasing dose from 50 to 300 μg/mL, while a similar trend was also observed in other two samples. When the concentration increased from 400 to 500 μg/mL, the OD ratio of these nanoparticles leaded to a slight decrease. It is worth pointing out that the biological effects of monodisperse and stable SiO_2 nanoparticles were excellent biocompatible and nontoxic.[40,41] In the present study, *in vitro* cytotoxicity further demonstrated that the ability of SiO_2@PAMC particles was found to possess non-cytotoxic and biocompatibility during 72 h incubation of cells. Meanwhile, Fig. 10(b–d) presents the corresponding optical images of L929 cells cultured in these samples with 300 μg/mL concentration for 72 h. The cells cultured in these samples exhibited normal morphological

characteristics after incubation, implying the favourable biocompatibility of the prepared nanoparticles. Therefore, the intrinsic biocompatibility, stable and high antibacterial activity make SiO_2@PAMC multilayer core–shell nanoparticles preferential candidates for application in water purification systems, food packaging, healthcare products, household sanitation, cosmetics, etc.

4. Conclusions

We presented an efficient and simple method for the design and fabrication of novel antimicrobial SiO_2@PAM nanoparticles with core–shell structure. To synthesize these antibacterial materials, silica nanoparticles was first synthesized as supports to enhance the activated surface, and then the developed surface modification process was achieved by LbL deposition of cationic and anionic PAMs on the silica surface via electrostatic self-assembly technique. After treatment with a bleach solution, the transformation of the amines groups in polymer shell made the manufacture of amine-type N-halamine nanoparticles a reality. Due to the coordinated effects of silica nanoparticles and polymeric N-halamine matrices, the resultant antibacterial core–shell material featured stable and high antibacterial activity toward both *S. aureus* and *E. coil*. Also, the synthesized nanoparticles were found to be non-cytotoxic and adaptable biocompatibility in the cell culture assessment. Therefore, such SiO_2@PAM core–shell material with PAM-deposited silica nanoparticeles may serve as practical and powerful antibacterial tools for bacterial infection-relative applications.

Acknowledgments

We acknowledge financial support from Zhejiang Provincial Natural Science Foundation of China (LY14E030014), Zhejiang Top Priority Discipline of Textile Science and Engineering (2015YXQN02), the Department of Education of Zhejiang Province (Y201534618), and the Outstanding Postgraduate Dissertation Growth Foundation of Zhejiang Sci-Tech University (2015YSPY37).

Electronic supplementary information (ESI) available

The photographs showing the bacterial culture plates of *S.aureus* upon the exposure to SiO_2@PAMC nanoparticles before storage at different contact time. See the appendix file.

Notes and references

1 Y. Zhou, X. Jiang, J. Tang, Y. Su, F. Peng, Y. Lu, R. Peng and Y. He, *J. Mater. Chem. B*, 2014, **2**, 691–697.

2 I. Cerkez, H. B. Kocer, S. D. Worley, R. M. Broughton, T. S. Huang, *React. Funct. Polym.*, 2012, **72**, 673–679.

3 Y. Chen, Q. Han, *Appl. Surf. Sci.*, 2011, **257**, 6034–6039.

4 Y. Sun, G. Sun, *Ind. Eng. Chem. Res.*, 2004, **43,** 5015–5020.

5 H. B. Kocer, I. Cerkez, S. D. Worley, R. M. Broughton, T. S. Huang, *ACS Appl. Mater. Interfaces*, 2011, **3**, 3189–3194.

6 E. Kenawy, S. D. Worley, R. Broughton, *Biomacromolecules*, 2007, **8**, 1359–1384.

7 L. Wu, Y. Xu, L. Cai, X. Zang, Z. Li, *Appl. Surf. Sci.*, 2014, **314**, 832–840.

8 X. H. Ren, A. Akdag, H. B. Kocer, S. D. Worley, R. M. Broughton, T. S. Huang, *Carbohydr. Polym.*, 2009, **78**, 220–226.

9 I. Cerkez, H. B. Kocer, S. D. Worley, R.M. Broughton, T.S. Huang, *React. Funct. Polym.*, 2012, **72**, 673–679.

10 A. Akdag, M. L. McKee, S. D. Worley, *J. Phys. Chem. A*, 2006, **110**, 7621–7627.

11 A. Dong, Y. Sun, S. Lan, Q. Wang, Q. Cai, X. Qi, Y. Zhang, G. Gao, F. Liu, C. Harnoode, *ACS Appl. Mater. Interfaces*, 2013, **5**, 8125–8133.

12 J. Jang, Y. Kim, *Chem. Commun.*, 2008, 4016–4018.

13 X. Ren, A. Akdag, C. Zhu, L. Kou, S. D. Worley, T. S. Huang. *J. Biomed. Mater. Res. A*, 2009, **91**, 385–390.

14 A. Dong, Z. Huang, S. Lan, Q. Wang, S. Bao, Siriguleng, Y. Zhang, G. Gao, F. Liu, C. Harnoode, *J. Colloid. Interface. Sci.*, 2014, **431**, 92–99.

15 A. Dong, Q. Zhang, T. Wang, W. Wang, F. Liu, G. Gao, *J. Phys. Chem. C*, 2010, **114**, 17298–17303.

16 B. Song, C. Wu, J. Chang, *Acta. Biomater.*, 2012, **8**, 1901–1907.

17 G. S. Alvarez, C. Hélary, A. M. Mebert, X. Wang, T. Coradin, M. F. Desimone, *J. Mater. Chem. B*, 2014, **2**, 4660–4670.

18 D. Gao, Z. Zhang, M. Wu, C. Xie, *J. Am. Chem. Soc.*, 2007, **129**, 7859–7866.

19 T. V. Podust, T. V. Kulik, B. B. Palyanytsya, V. M. Gunko, A. Tóth, L. Mikhalovska, A. Menyhárd, K. László, *Appl. Surf. Sci.*, 2014, **320**, 563–569.

20 Y. Yang, X. Song, Y. Yao, H. Wu, J. Liu, Y. Zhao, M. Tan, Q. Yang, 2015, DOI: 10.1039/c5tb00398a.

21 M. Karg, T. Hellweg, *J. Mater. Chem.*, 2009, **19**, 8714–8727.

22 J. Song, H. Song, H. Kong, J. Hong, J. Jang, *J. Mater. Chem.*, 2011, **21**, 19317–19323.

23 A. Dong, J. Huang, S. Lan, T. Wang, L. Xiao, W. Wang, T. Zhao, X. Zheng, G. Gao, Y. Chen, *Nanotechnology*, 2011, **22**, 295602.

24 R. Palkovits, H. Althues, A. Rumplecker, B. Tesche, A. Dreier, U. Holle, G. Fink, C. H. Cheng, D. F. Shantz, S. Kaskel, *Langmuir*, 2005, **21**, 6048–6053.

25 H. Sertchook, D. Avnir, *Chem. Mater.*, 2003, **15**, 1690–1694.

26 H. Zhou, T. Shi, X. Zhou, *Appl. Surf. Sci.*, 2013, **266**, 33–38.

27 W. Stöber, A. Fink, E. Bohn, *J. Colloid. Interface. Sci.*, 1968, **26**, 62–69.

28 Q. Zhang, A. Dong, Y. Zhai, F. Liu and G. Gao, *J. Phys. Chem. C*, 2009, **113**, 12033–12039.

29 C. Li, J. Hou, Z. Huang, T. Zhao, L. Xiao, G. Gao, C. Harnoode, A. Dong, *Colloid. Surf. B. Biointerfaces.*, 2015, **126**, 106–114.

30 T. Yao, Q. Lin, K. Zhang, D. Zhao, H. Lv, J. Zhang and B. Yang, *J. Colloid. Interface. Sci.*, 2007, **315**, 434–438.

31 M. K. Krušić, E. Džunuzović, S. Trifunović, J. Filipović, *Eur. Polym. J.*, 2004, **40**, 793–798.

32 K. Zhang, Q. Wang, H. Meng, M. Wang, W. Wu, J. Chen, *Particuology*, 2014, **14**, 12–18.

33 E. Meaurio, I. Katime, *Macromol. Mater. Eng.*, 2005, **290**, 1166–1175.

34 Y. Zhao, Y. Chen, M. Li, S. Zhou, A. Xue, W. Xing, *J. Hazard. Mater.*, 2009, **171**, 640–646.

35 C. D. Schmulbach, R. S. Drago, *J. Phys. Chem.*,1960, **64**, 1956–1958.

36 S. Hayakawa, L. L. Hench, *J. Non-Cryst. Solids.*, 2000, **262**, 264–270.

37 T. Liu, X. Ding, X. Yang, Z. Gou, J. Chen, X. Feng, *J. Non-Cryst. Solids.*, 2014, **389**, 104–112.

38 K. Barnes, J. Liang, R. Wu, S. D. Worley, J. Lee, R. M. Broughton, T. S. Huang, *Biomaterials*, 2006, **27**, 4825–4830.

39 H. B. Kocer, S. D. Worley, R. M. Broughton, T. S. Huang, *React. Funct. Polym.*, 2011, **71**, 561–568.

40 M. A. Malvindi, V. Brunetti, G. Vecchio, A. Galeone, R. Cingolani, P. Pompa, *Nanoscale*, 2012, **4**, 486–495.

41 Y. S. Li, J. L. Shi, *Adv. Mater.*, 2014, **26**, 3176–3205.

Figure captions

Figure. 1 Schematic illustration for the formation processes of SiO_2@PAM core–shell nanoparticles.

Figure. 2 TEM and FESEM images of (a and b) pure SiO_2 and (d and e) SiO_2@PAM core–shell nanoparticels; corresponding size distribution of (c) pure SiO_2 and (f) SiO_2@PAM core–shell nanoparticels. The insert of FESEM images showing the corresponding particle size.

Figure. 3 DSC curves of pure SiO_2 and SiO_2@PAM nanoparticles.

Figure. 4 TGA curves of pure SiO_2, CPAM, and SiO_2@PAM samples.

Figure. 5 FTIR spectra of pure SiO_2, pure CPAM, SiO_2@PAM, and SiO_2@PAMC nanoparticles.

Figure. 6 UV-vis absorption spectra of pure SiO_2, SiO_2@PAM, and SiO_2@PAMC nanoparticles.

Figure. 7 Antibacterial photographs (a) of the culture plates of *E. coli* and *S. aureus* exposure to pure SiO_2, SiO_2@PAM, and SiO_2@PAMC nanoparticles. (b) Quantitative evaluation of the antimicrobial ability of the synthesized nanoparticles by counting the colonies grown on agar plates.

Figure. 8 Antibacterial activity of samples. Turbidity photographs of the test tubes against Gram-negative bacteria *E. coli* (a) and Gram-positive bacteria *S. aureus* (b). Bacterial growth curves of *E. coli* (c) and *S. aureus* cells (d) in LB media. The growth of the bacteria is measured by the OD at 600 nm wavelength.

Figure. 9 Photographs showing the bacterial culture plates of *S.aureus* upon the exposure to SiO_2@PAMC nanoparticles after storage under different contact time: (a) control, (b) 5 min, (c) 15 min, (d) 30 min, and (e) 60 min. (f) Antibacterial kinetic test graphs for SiO_2@PAMC nanoparticles against *S. aureus* as a function of contact time before and after two month storage.

Figure. 10 Cytotoxicity of the prepared nanoparticles. (a) Viability of L929 cells incubated with SiO_2, SiO_2@PAM, and SiO_2@PAMC nanoparticles with different concentrations for 72 h (* indicates significant difference compared to SiO_2 group, $p < 0.05$). Optical images of L929 cells cultured in SiO_2 (b), SiO_2@PAM (c), SiO_2@PAMC (d) samples with 300 μg/mL concentration for 72 h.

Fig. 1 Schematic illustration for the formation processes of SiO_2@PAM core–shell nanoparticles.

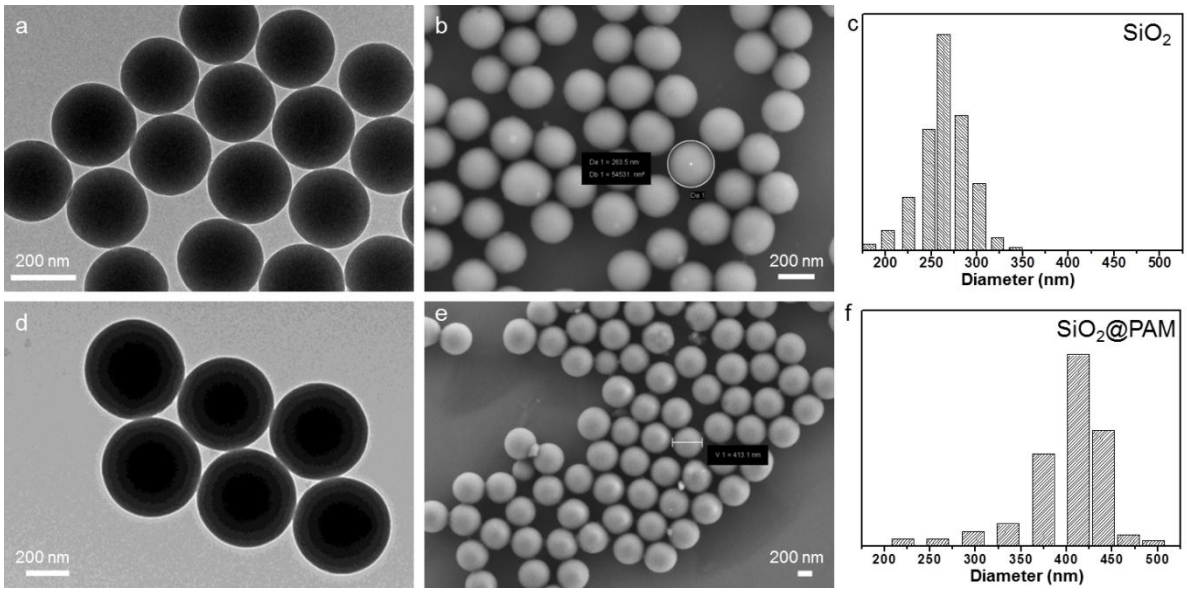

Fig. 2 TEM and FESEM images of (a and b) pure SiO_2 and (d and e) SiO_2@PAM core–shell nanoparticels; corresponding size distribution of (c) pure SiO_2 and (f) SiO_2@PAM core–shell nanoparticels. The insert of FESEM images showing the corresponding particle size.

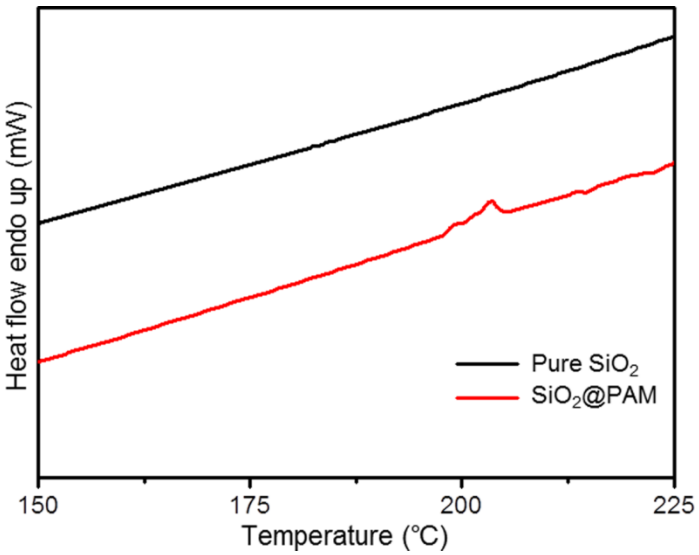

Fig. 3 DSC curves of pure SiO_2 and SiO_2@PAM nanoparticles.

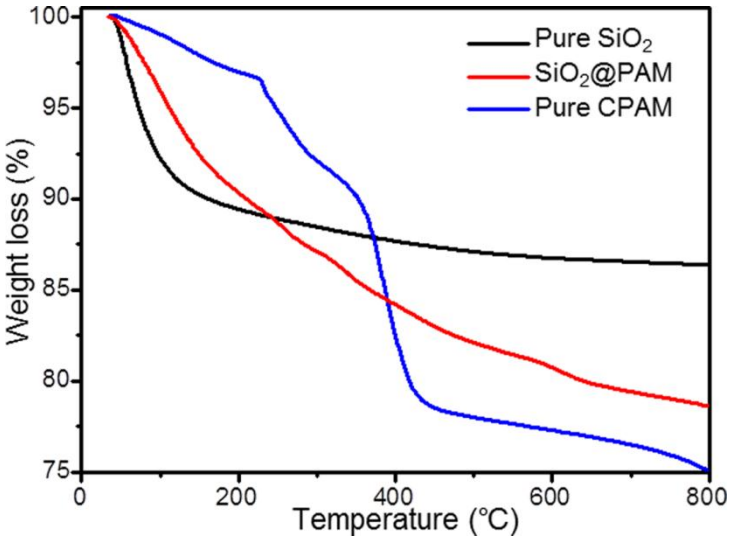

Fig. 4 TGA curves of pure SiO_2, CPAM, and SiO_2@PAM samples.

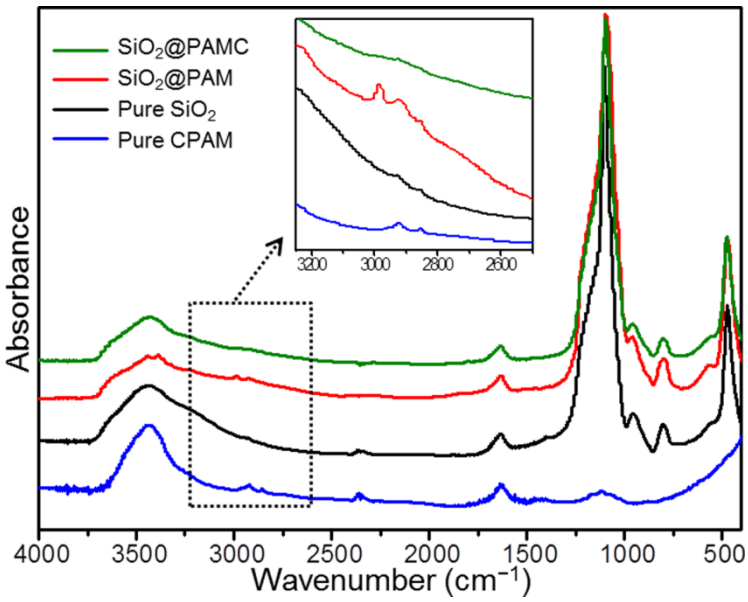

Fig. 5 FTIR spectra of pure SiO_2, pure CPAM, SiO_2@PAM, and SiO_2@PAMC nanoparticles.

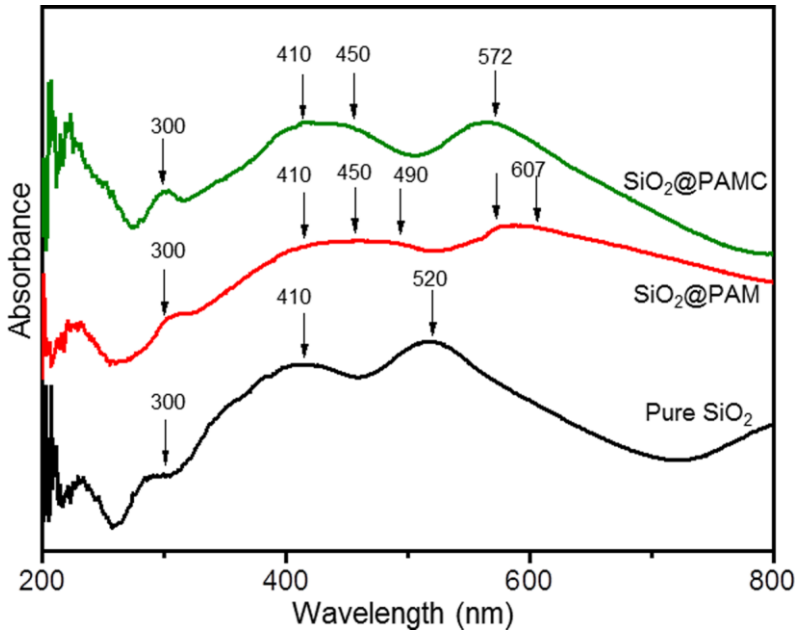

Fig. 6 UV-vis absorption spectra of pure SiO_2, SiO_2@PAM, and SiO_2@PAMC nanoparticles.

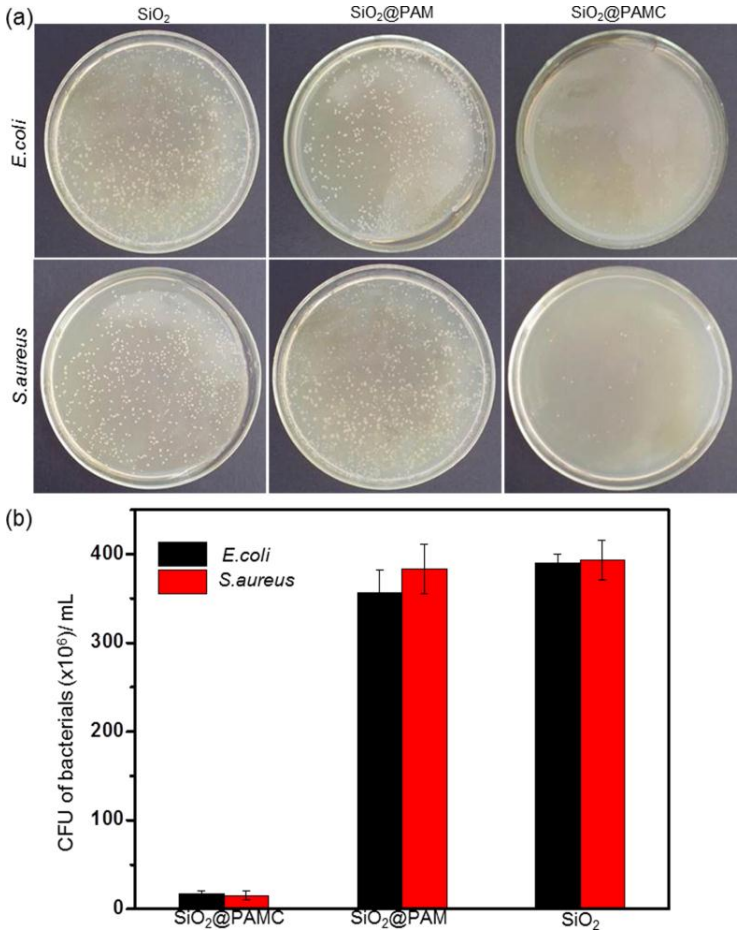

Fig. 7 Antibacterial photographs (a) of the culture plates of *E. coli* and *S. aureus* exposure to pure SiO_2, SiO_2@PAM, and SiO_2@PAMC nanoparticles. (b) Quantitative evaluation of the antimicrobial ability of the synthesized nanoparticles by counting the colonies grown on agar plates.

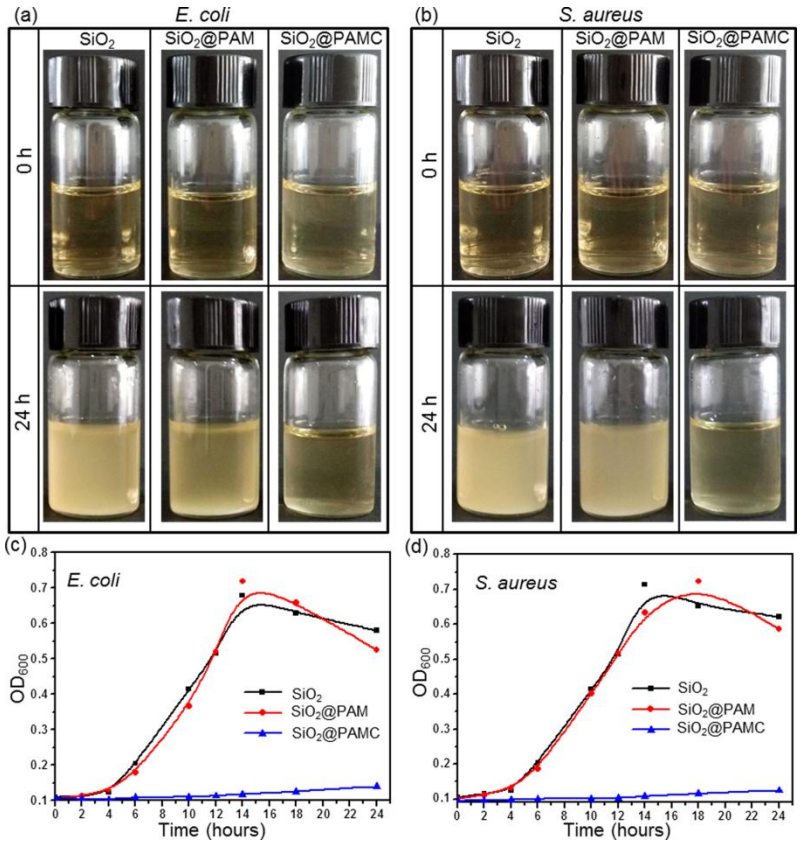

Fig. 8 Antibacterial activity of samples. Turbidity photographs of the test tubes against Gram-negative bacteria *E. coli* (a) and Gram-positive bacteria *S. aureus* (b). Bacterial growth curves of *E. coli* (c) and *S. aureus* cells (d) in LB media. The growth of the bacteria was measured by the OD at 600 nm wavelength.

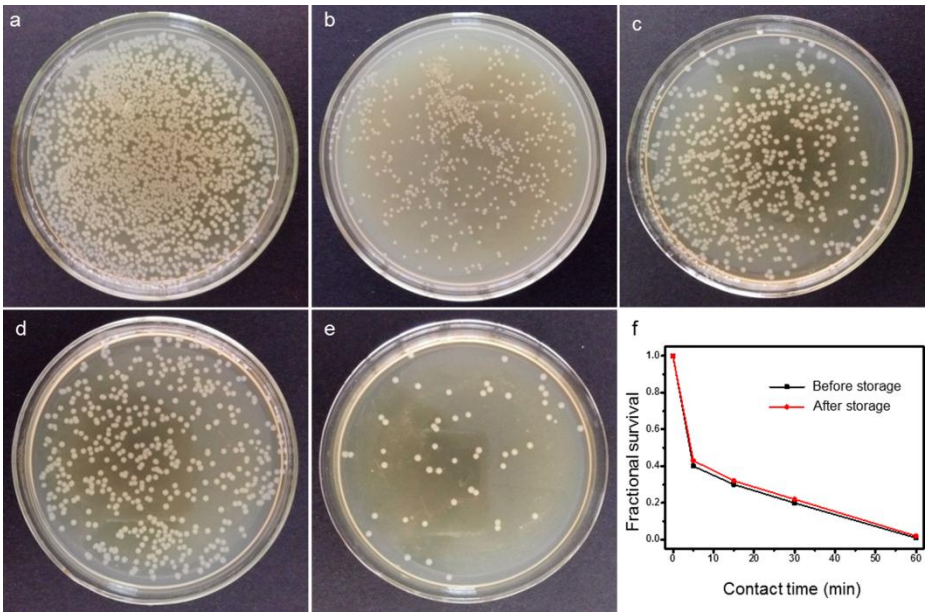

Fig. 9 Photographs showing the bacterial culture plates of *S.aureus* upon the exposure to SiO_2@PAMC nanoparticles under different contact time: (a) control, (b) 5 min, (c) 15 min, (d) 30 min, and (e) 60 min. (f) Antibacterial kinetic test graphs for SiO_2@PAMC nanoparticles against *S. aureus* as a function of contact time before and after two month storage.

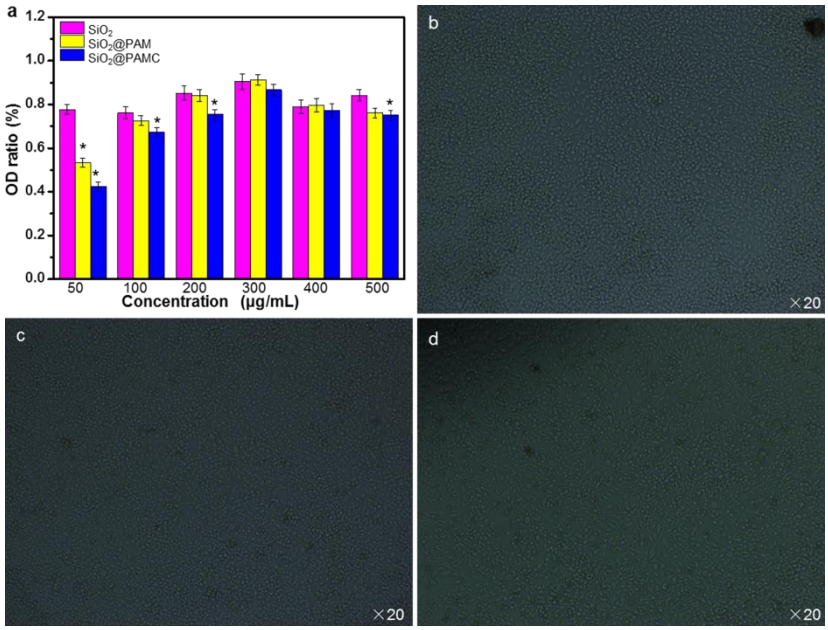

Fig. 10 Cytotoxicity of the prepared nanoparticles. (a) Viability of L929 cells incubated with SiO_2, SiO_2@PAM, and SiO_2@PAMC nanoparticles with different concentrations for 72 h (* indicates significant difference compared to SiO_2 group, $p < 0.05$). Optical images of L929 cells cultured in SiO_2 (b), SiO_2@PAM (c), SiO_2@PAMC (d) samples with 300 μg/mL concentration for 72 h (×20 magnification).

Graphical Abstract

Monodisperse multilayer core–shell nanoparticles with outer antimicrobial PAM shell-decorated inner SiO_2 core were fabricated using layer-by-layer electrostatic self-assembly technique; they exhibited excellent antibacterial activities against gram-positive bacteria as well as gram-negative bacteria.